

# Electric field dependent thermal conductivity of relaxor ferroelectric PMN-33PT through changes in the phonon spectrum

*Delaram Rashadfar<sup>1</sup>, Brandi L. Wooten<sup>2\*</sup>, Joseph P. Heremans<sup>1,2,3\*</sup>*

1. Department of Mechanical and Aerospace Engineering, Ohio State University, Columbus OH 43210, USA
2. Department of Materials Science and Engineering, Ohio State University, Columbus OH 43210, USA
3. Department of Physics, Ohio State University, Columbus OH 43210, USA

E-mail: Wooten.120@osu.edu, Heremans.1@osu.edu

\* co-corresponding authors

Keywords: polarization caloritronics, ferroelectric-relaxors, thermal conductivity, sound velocity, piezoelectric coefficients; heat switches.

## Abstract

In ferroelectric materials, an applied electric field has been shown to change the phonon dispersion relation sufficiently to alter the lattice thermal conductivity, opening the theoretical possibility that a heat gradient could drive a polarization flux, and technologically, also opening a new avenue toward all solid-state heat switching. In this report, we confirm experimentally the validity of the theory originally developed for  $Pb(Zr,Ti)O_3$  (PZT) on the ferroelectric relaxor  $0.66Pb[Mg_{1/3}Nb_{2/3}]O_3 - 0.33PbTiO_3$  (PMN-33PT). In the theory, the relative change in sound velocity and thermal conductivity with applied electric field relates to the piezoelectric coefficients ( $d_{33}$  and  $d_{31}$ ) and the Grüneisen parameter ( $\gamma$ ). The theory predicts that in PMN-33PT the effect should be an order of magnitude larger, and of opposite sign as in PZT; this is confirmed here. The effect is measured on samples that undergo multiple field sweep cycles and pass through 2 phase transitions. The thermal conductivity changes are closely linked to variations in the piezoelectric coefficients. A null experiment on paraelectric  $SrTiO_3$  confirms the link between ferroelectricity and phonon spectrum changes. Changes in heat conduction as large as 10% can be achieved over large temperature ranges, opening a possibility for practical heat switches based on phonon spectrum changes.

## 1. Introduction

The fact that an electric field can alter the phonon spectrum and heat propagation in ferroelectric materials, and the Onsager reciprocal of this concept, namely that a temperature gradient may drive a current of polarization, opens the possibility of a new field of physics, *polarization caloritronics*.<sup>[1]</sup> With increasing temperature, the saturation polarization  $P_S$  of ferroelectric (FE) materials decreases ( $\frac{dP_S}{dT} < 0$ ), much like the saturation magnetization  $M_S$  in ferromagnetic (FM) materials ( $\frac{dM_S}{dT} < 0$ ). In FMs, this effect is due to the increasing number of spin precession waves, quasiparticles known as magnons. In FEs, it is due to the increasing number of phonons that involve the motion of the ions that carry the charges that gives rise to the individual dipole moments in each lattice unit; Bauer et al.<sup>[2]</sup> labels this subset of phonons as *ferrons*. Since  $\frac{dM_S}{dT} < 0$ , a temperature gradient implies the existence of a temperature-driven spin flux in FMs; it is therefore logical to consider that FEs host temperature-driven polarization fluxes. This concept, polarization caloritronics, is rich in consequences as it paves the way toward a slew of new possible applications in heat switches, thermoelectric concepts, and even phonon-based logic.<sup>[1]</sup> The first experimental result in this field by Wooten et al.<sup>[3]</sup> is a measurement of the electric field dependency of thermal conductivity, thermal diffusivity, electric susceptibility, and the longitudinal-mode sound velocity of FE  $Pb(Zr,Ti)O_3$  (PZT). That work demonstrated that ferrons are not only optical phonons, but also propagating acoustic phonons that are strain-coupled to optical phonons.

A quantitative theory<sup>[3]</sup> for the effect with no adjustable parameters relates changes in the sound velocity  $v$  to the piezoelectric coefficients  $d_{33}$  and  $d_{31}$  and the Grüneisen parameter  $\gamma$ . The piezoelectric coefficients are defined as  $d_{33} = \frac{\partial e_{33}}{\partial E}$  and  $d_{31} = \frac{\partial e_{11}}{\partial E}$ , where  $e_{33(11)}$  is the strain tensor component that gives the compression or expansion along (perpendicular to) the direction of ferroelectric order, which is parallel to the applied field  $E = E_3$ . The mode ( $i$ ) and wavevector ( $k$ ) dependent Grüneisen parameter is the logarithmic derivative of that phonon mode's frequency vis-à-vis the volume  $V$  of the sample,  $\gamma(i, k) = \frac{d \ln(\omega_{i,k})}{d \ln(V)}$ , by definition. For longitudinal or transverse acoustic phonons ( $i = LA$  or  $TA$ , respectively), this gives  $\gamma(i) = \frac{d \ln(v_i)}{d \ln(V)}$ . The basis of the theory is to first describe how the piezoelectric coefficients relate the change in volume of the

sample with applied field to  $(d_{33} + 2d_{31})$  and then relate that to the logarithmic derivative of the sound velocity for each mode:

$$\frac{v'}{v_0} = \frac{d \ln(v)}{dE} = -\gamma(d_{33} + 2d_{31}) \quad (1)$$

Here,  $v' = \frac{dv}{dE}$  is the derivative of the sound velocity with respect to the applied electric field and  $\gamma$  is the specific heat-weighted mode and wavevector average of  $\gamma(i, k)$ . From the sound velocity we move to the thermal conductivity using the equation  $\kappa = \frac{1}{3} C v l = \frac{1}{3} C v^2 \tau$ , where  $C$  represents the volumetric specific heat,  $l$  the mean free path and  $\tau$  the relaxation time;  $v$  here is the average velocity of the LA and 2 TA modes. At temperatures above the Debye temperature, the specific heat is constant with  $E$ , being a function of only  $T$  and the number of atoms per unit volume  $n$ ,  $C = 3n k_B T$  ( $k_B$  is the Boltzmann constant). Assuming that the relaxation time is independent of electric field, we can relate the electric field dependency of both the sound velocity and thermal conductivity  $\kappa$  above the Debye temperature as:

$$\frac{\kappa'}{\kappa_0} = \frac{2v'}{v_0} \quad (2)$$

where again  $\kappa' = \frac{d\kappa}{dE}$ . The validity of **Equations (1)** and **(2)** was tested experimentally on PZT and confirmed in Wooten et al.<sup>[3]</sup> without the use of adjustable parameters since  $d_{33}$ ,  $d_{31}$  and  $\gamma$  were known. If this theory has predictive value, it allows us to sort amongst known ferroelectrics for the compound that has the largest field dependence of thermal conductivity, and is thus most useful in thermal switching applications.

Heat switches, or thermal transistors, are a particularly useful element in heat management,<sup>[4]</sup> which is key to the continued scaling up of the complexity in advanced semiconductor integrated circuits. They are also the key element in all-solid-state power generation and refrigeration cycles based on electrocaloric and magnetocaloric effects, where no fluid is circulated but only heat. Many heat switching technologies exist,<sup>[5]</sup> including one that is based on domain wall motion in ferroelectrics;<sup>[6]</sup> however, the mechanism here, phonon spectrum shifts, promises to give reasonable effects over a large temperature range if maximized. Ultimately, the goal is to create a thermal switch with the largest switching ratio. **Equation 1** sheds light on the

material parameters needed to maximize this effect – very anharmonic phonons denoted by a large Grüneisen parameter  $\gamma$  and maximization of the summation ( $d_{33} + 2d_{31}$ ).

We found one: the relaxor ferroelectric system  $Pb[Mg_{1/3}Nb_{2/3}]O_3 - PbTiO_3$  (PMN-PT) of the composition  $0.66Pb[Mg_{1/3}Nb_{2/3}]O_3 - 0.33PbTiO_3$  (PMN-33PT) on which predicted an effect an order of magnitude larger and of opposite sign from that in PZT, based on the literature values of  $d_{33}$ ,  $d_{31}$  and  $\gamma$ . In this manuscript, we report this prediction to be experimentally true in fresh samples, but we surprisingly found that samples that were subjected to multiple cycles of poling and depoling showed an even larger effect and another sign change, ultimately due to changes in the piezoelectric constants. We explore the behavior of  $\kappa'/\kappa_0$  over the different crystallographic phases of PMN-33PT with temperature. Finally, we also provide the null experiment by reporting an essentially zero  $\kappa'/\kappa_0$  and  $\nu'/\nu_0$  for paraelectric  $SrTiO_3$  proving that ferroelectricity is needed for this behavior. This paper therefore gives additional proof that ferrons can be propagating acoustic phonons, and thus, by Onsager reciprocity,<sup>[2]</sup> that a heat-driven polarization flux must exist.

## 2. PMN-PT

The relaxor ferroelectric PMN-PT has gained significant attention for its enhanced piezoelectric properties and, as such, is the obvious choice of material to investigate for a large field enhanced thermal conductivity. PMN-PT is a relatively complex material system undergoing a surge of research into its properties as a function of electric field,<sup>[7-10]</sup> temperature,<sup>[7-12]</sup> phase composition,<sup>[13-15]</sup> poling direction,<sup>[15,16]</sup> poling method (AC or DC, frequency of AC, etc.),<sup>[17]</sup> synthesis methods, and chemical composition<sup>[15,18]</sup> due to its unusually large piezoelectric and electromechanical properties.

PMN-PT is a relaxor ferroelectric, a solid solution of a disordered relaxor (PMN) and a ferroelectric (PT) material defined as possessing a temperature-dependent and broadened dielectric permittivity peak. Relaxor ferroelectrics contain small islands of ferroelectric ordering, coined polar nano-regions (PNR), that exists within a paraelectric matrix; however, this is a controversial statement as some believe the matrix has ferroelectric order.<sup>[19]</sup> The morphotropic phase boundary of  $PMN_{1-x}PT_x$  is close to  $x = 0.35$ . Below this composition, the primary structure is rhombohedral,

and above this composition, the primary structure is tetragonal. The polarization of this system is complex as it accompanies a crystallographic phase transition that depends on both temperature and electric field.<sup>[20]</sup>

## 2.1 Experiments

The compound we use here is PMN-33PT ( $x = 0.33$ ) in single-crystal form. It goes through several crystallographic phase transitions as a function of field and electric field.<sup>[7]</sup> At zero field, it is tetragonal (T) above about 320 K and monoclinic (M) below. The M phase contains two sub-phases,  $M_A$  and  $M_C$ , where the subscript denotes different polarization vector directions. The phases are readily apparent in thermal conductivity measurements at zero field with the heat flux applied along the (100) direction, reported in **Figure 1**.

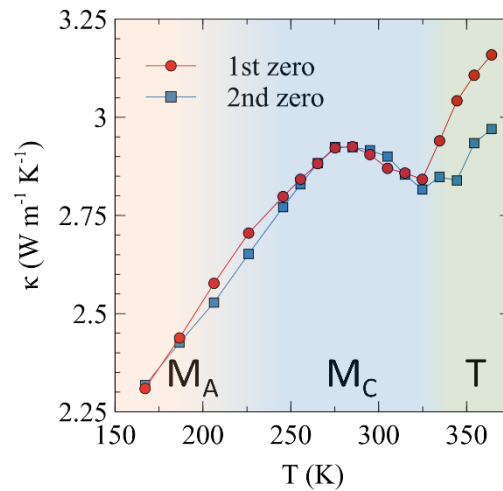


**Figure 1.** Temperature dependent phase transitions observed in thermal conductivity measurements at zero field. In the legend, ‘1<sup>st</sup> zero’ refers to the thermal conductivity value at zero field as the swept field is decreasing, and ‘2<sup>nd</sup> zero’ refers to the value at zero field as the swept field is increasing.  $M_A$ ,  $M_C$ , and T refer to the two monoclinic and tetragonal phases that PMN-33PT passes through as the temperature changes.

Below ~225 K, PMN-33PT exists in the  $M_A$  phase, transitioning to the  $M_C$  phase between ~225 K and ~325 K. Beyond ~325 K, it adopts a T structure. Notably, as no electric field is applied at this time, the observed phase transitions solely occur because of temperature variations.

These phases are also dependent on the electric field. For example, if the sample is slightly above room temperature, it can transition from  $M_A$  to  $M_C$  with increasing field. These transitions are obvious in the strain vs electric field curves found in Reference Davis et al.<sup>[7]</sup> Ultimately, these transitions are a function of temperature, electric field, synthesis protocols, composition, and poling conditions.<sup>[7-17]</sup> For example, PMN-33PT has a large piezoelectric coefficient  $\sim d_{33}=1500$  pC N<sup>-1</sup>;<sup>[20]</sup> a recent paper<sup>[17]</sup> related the poling conditions to  $d_{33}$  and found that  $d_{33}$  can change drastically with the poling electric field strength and AC or DC poling conditions. These materials have many desired properties but are complex in nature which leads to some ambiguity in measurements and results in the literature.

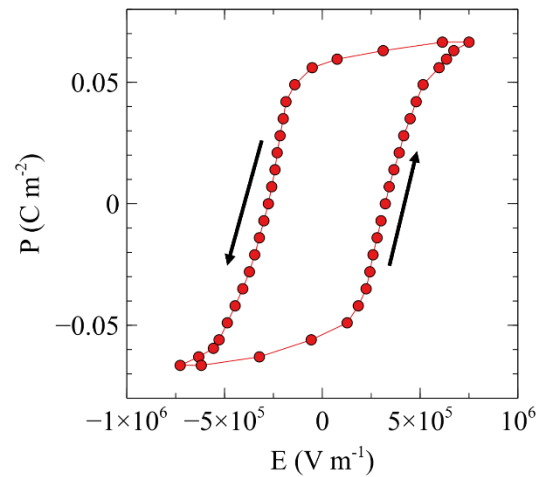


**Figure 2.** Polarization of PMN-33PT at room temperature. Arrows indicate the direction of the swept field.

The polarization vs electric field along the (001) direction results at room temperature are shown in **Figure 2**. The coercive field is about  $3 \times 10^5$  V m<sup>-1</sup> and the saturation field is about  $6 \times 10^5$  V m<sup>-1</sup> with a polarization of about  $0.06$  C m<sup>-2</sup>.

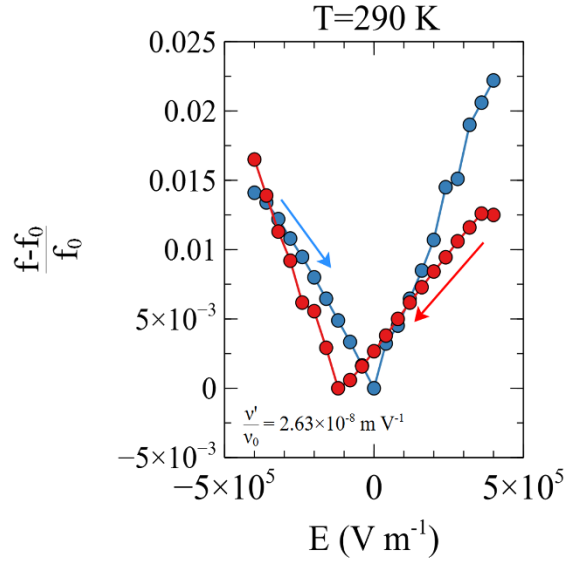


**Figure 3.** Resonant Ultrasound Spectroscopy (RUS) measurement results of the frequency of the longitudinal compressive mode on a parallelepiped sample of PMN-33PT at 290 K. The relative change of this longitudinal resonant frequency is tracked as a function of electric field. The relative change of frequency equals the relative change of  $v'/v_0$  of the longitudinal acoustic phonon along the (100) direction of the crystal.

**Figure 3** shows the result of Resonant Ultrasound Spectroscopy (RUS) taken on a sample of PMN-33PT as function of an electric field applied along the (001) direction. The RUS measures the frequency  $f$  of the resonance of the longitudinal compressive mode of the whole sample along the (100) direction. The relative change of this frequency with applied electric field,  $(f(E) - f_0)/f_0$ , shown in **Figure 3**, was taken on a fresh sample at  $\sim 290$  K by applying DC voltage from the maximum positive field to zero and then from zero to the maximum negative field and vice versa. The peak around 320 kHz, corresponding to the longitudinal resonant frequency, was tracked as a function of electric field.  $f_0$  corresponds to the zero-field value. Because both the resonant frequency and the sound velocity are proportional to square roots of the elastic constant  $c_{11}$ ,  $1/f_0 \frac{df(E)}{dE} = v'/v_0$  where  $v$  is the sound velocity of the longitudinal acoustic phonon along the (100) direction. Thus, we calculate the relative field dependence of the sound velocity of this phonon  $v'/v_0$  to be  $2.63 \times 10^{-8} \text{ m V}^{-1}$ .

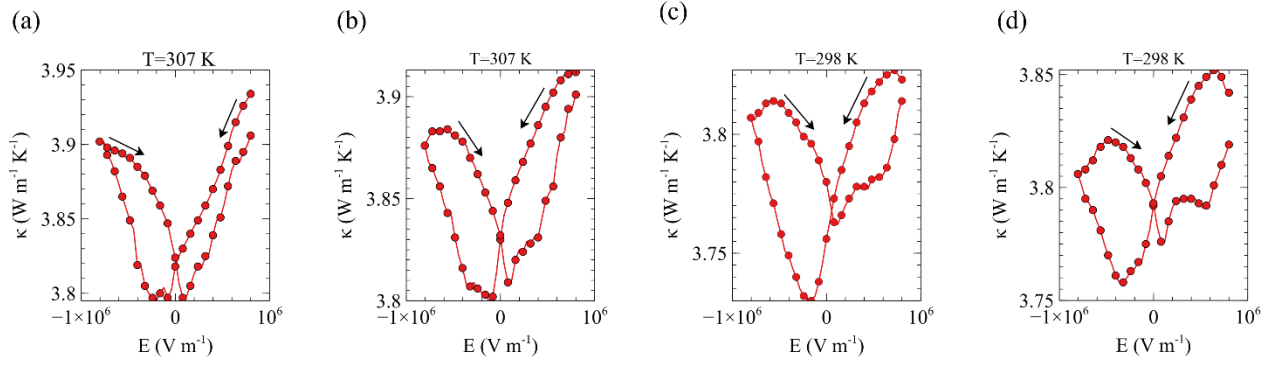


**Figure 4.** a-d) Thermal conductivity measurements around room temperature on a fresh PMN-33PT sample: (a) the first run, (b) the second run, (c) the third run, and (d) the fourth run of sweeping field. The arrows indicate the direction of sweep.

**Figures 4a-d** display the thermal conductivity of the first PMN-33PT sample at 298 K and 307 K on the first, second, third, and fourth sweep of the electric field. The experimental values of thermal conductivity for sample 1 are mentioned in **Table 1**. The point worth noting is that they are all in the same order of magnitude, but  $\kappa'/\kappa_0$  decreases sharply by the fourth sweep in the electric field.

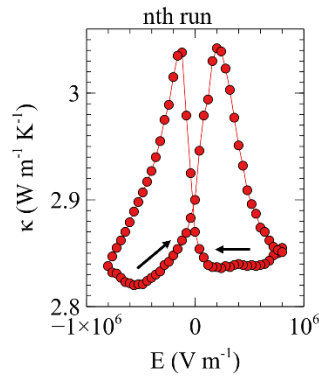


**Figure 5.** Room temperature thermal conductivity measurements on the second PMN-33PT sample that was cycled through electric field multiple ( $n > 10$ ) times. The arrows indicate direction of sweep. This result is stable vis-à-vis subsequent electric field cycles.



**Figure 5** illustrates the behavior of the second sample after subjecting it to over 10 electric field sweeps. By contrasting the first few runs on the first sample shown in **Figures 4a-d** with the results from the sample swept more than 10 times in **Figure 5**, we see how the thermal conductivity changes indicating a transition. This transition is stable, and the trend in **Figure 5** does not change with further electric field or temperature cycling.

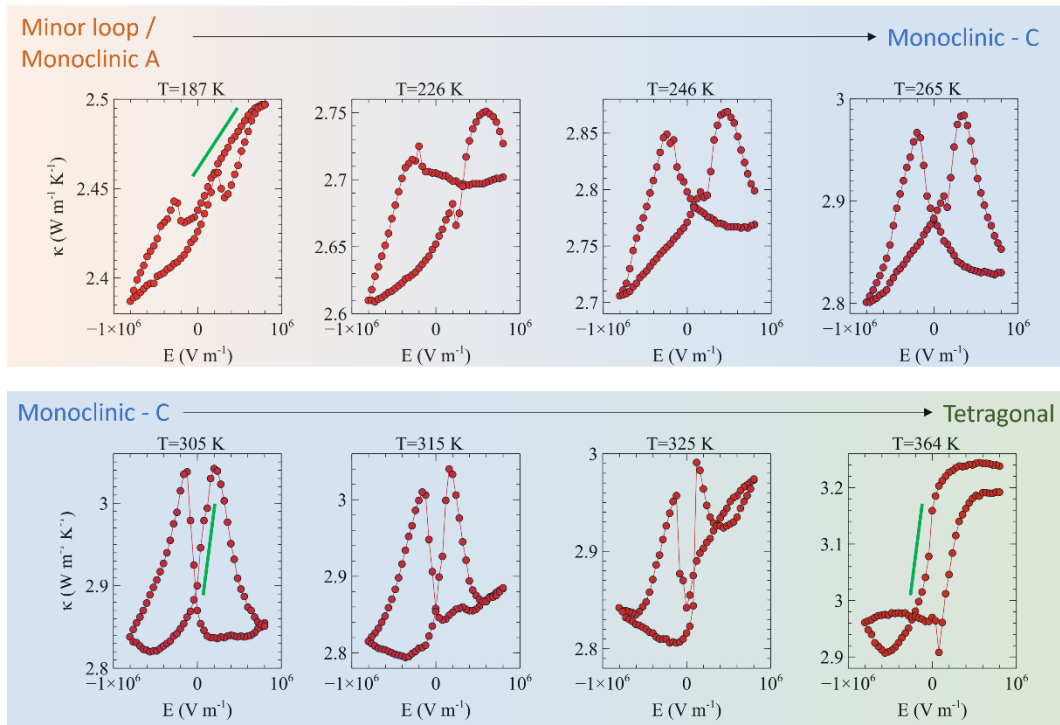


**Figure 6.** Thermal conductivity measurements at different temperatures on the second PMN-33PT sample under electric field. At cooler temperatures, we are in the monoclinic A phase; however, we may also be on a minor loop as the field may not be strong enough at this temperature to reach saturation. Around 265 to 315 K, we are in the monoclinic C phase, and we see symmetric curves with loop closure. Upon heating up to 364 K, we move to the tetragonal phase. Here, we see the greatest switching ratio. The green lines in the  $T=187$ , 305, and 365 K plots indicate where the slope was taken to calculate the values shown in **Table 1**.

**Figure 6** shows how thermal conductivity changes as a function of electric field at different temperatures on the second sample. At the lower temperature  $T=187$  K, we see an odd function of field but with hints of peaks at the coercive field. This observed trend could be indicative of a distinct phase; however, it is likely that we are on a minor loop and cannot safely apply enough voltage to saturate the polarization in the experiment. As the temperature increases, broader peaks begin to form at the coercive field values, until we see a symmetric even function of field at 265 K. This trend persists until about 315 K. Upon further heating, the thermal conductivity shifts to an odd function of field with observed saturation at the higher fields.

All these observations are summed up in **Table 1** that shows the  $\kappa'/\kappa_0$  values for the first four runs on the first sample around room temperature and the second sample at 187, 305, and 364 K. Runs 1, 2, 3, and 4 correspond with the plots shown in **Figures 4a-d** and the second samples correspond to those shown in **Figure 6** with appropriate temperature labels. The first run gives a  $\kappa'/\kappa_0$  of almost  $4 \times 10^{-8} \text{ m V}^{-1}$  but reduces to  $2.68 \times 10^{-8} \text{ m V}^{-1}$  by the fourth run. The second sample near room temperature ( $\kappa'/\kappa_0 = -3.86 \times 10^{-7} \text{ m V}^{-1}$ ) shows a sign flip and the signal is an order of magnitude larger than the first sample and two orders of magnitude larger than PZT ( $\kappa'/\kappa_0 = -7 \times 10^{-9} \text{ m V}^{-1}$ ).<sup>[3]</sup> The total change in thermal conductivity of sample 2 with field at higher temperatures is close to 10%. This sign change and magnitude proved to be irreversible and stable.

**Table 1.** Collected  $\kappa'/\kappa_0$  values from sample 1 with four runs around room temperature and sample 2 at various temperatures.

Sample	Phase	Temperature [K]	$\kappa'/\kappa_0$ [ $\text{m V}^{-1}$ ]
Sample 1 – Run 1	M <sub>C</sub>	307	$3.94 \times 10^{-8}$
Sample 1 – Run 2	M <sub>C</sub>	298	$3.00 \times 10^{-8}$
Sample 1 – Run 3	M <sub>C</sub>	307	$3.20 \times 10^{-8}$
Sample 1 – Run 4	M <sub>C</sub>	298	$2.68 \times 10^{-8}$
Sample 2	M <sub>A</sub> (Minor loop)	187	$-3.13 \times 10^{-8}$
Sample 2	M <sub>C</sub>	305	$-3.86 \times 10^{-7}$
Sample 2	T	364	$-2.61 \times 10^{-7}$

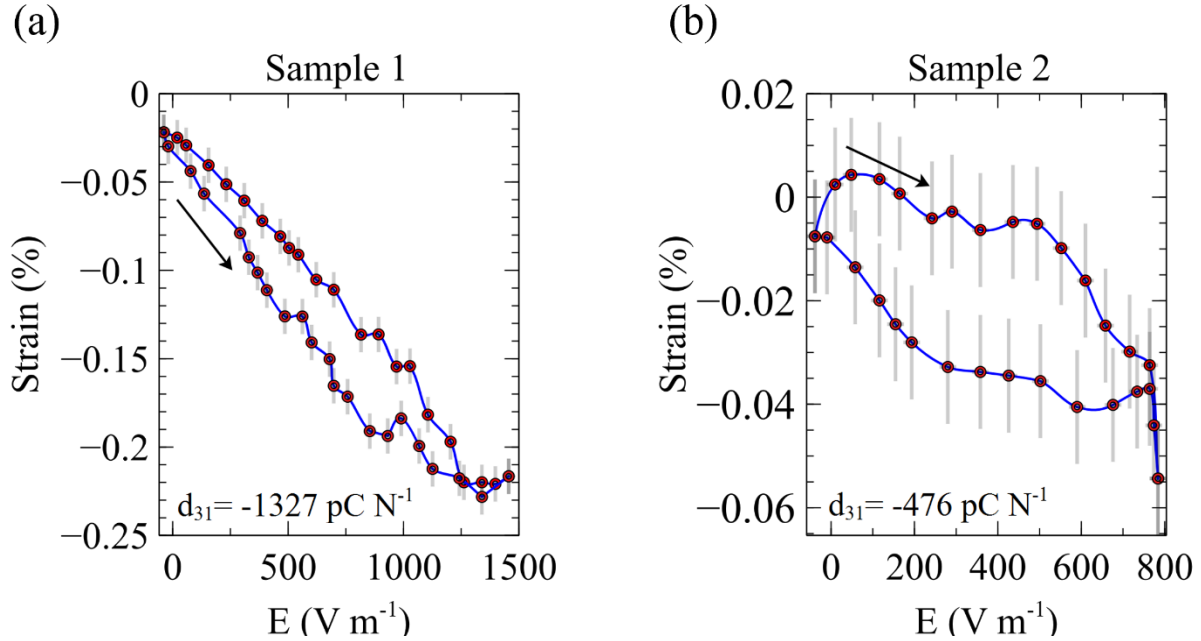


**Figure 7.** a-b) Piezoelectric strain measurements on the (a) first PMN-33PT sample and (b) second PMN-33PT sample. The slopes taken in decreasing field, indicated with arrows, were used to calculate the piezoelectric constant  $d_{31}$  values.

**Figure 7** illustrates  $d_{31}$  measurements on two distinct samples: one pristine, untouched by an electric field, and the other, a cycled sample previously employed for thermal conductivity measurements. To measure the transverse piezoelectric constant, we measured the change of the length of the sample along the (100) direction as a function of the electric field along the (001) direction. This change in the length of the sample corresponds to changes in the strain tensor; the derivative of these strain tensor components gives the piezoelectric coefficient. We calculated a  $d_{31}$  of  $-1327 \text{ pC N}^{-1}$  for the fresh sample and  $-476 \text{ pC N}^{-1}$  for the cycled sample, a reduction of nearly three times.

## 2.2 The null experiment on $\text{SrTiO}_3$ (STO)

The theory presented by Bauer et al.<sup>[2]</sup> and Wooten et al.,<sup>[3]</sup> does not make use of the remanent polarization, so it was unclear if ferroelectric ordering was necessary to have a ferronic

thermal conductivity. To test this, we conducted thermal conductivity and RUS measurements on paraelectric STO.

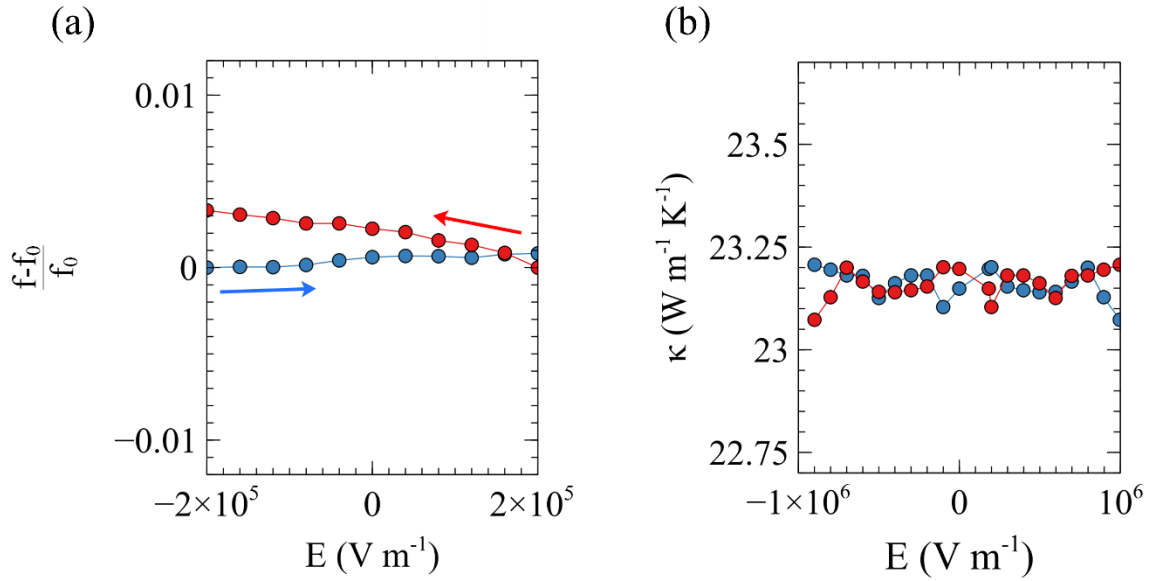


**Figure 8.** a-b) (a) RUS and (b) thermal conductivity measurements on a sample of  $SrTiO_3$  around room temperature.

**Figures 8a and b** show the RUS results and thermal conductivity measurements, respectively, on paraelectric STO at room temperature. We see almost no electric field dependency in either of the measurements. The slight slopes in the frequency tracking (**Figure 8a**) were probably drift due to fluctuations in the room temperature as this measurement was done at ambient pressure with no temperature control.

### 2.3 Theory

Applying **Equations (1) and (2)** to compare theory to the data above requires knowledge of  $\gamma$ ,  $d_{31}$  and  $d_{33}$ . The former is calculated to be  $\gamma=15$  for PZT,<sup>[21]</sup> the same value will be assumed here since  $PbTiO_3$  is presumably the active ingredient. The literature values of  $d_{33} = 1225 \text{ pC N}^{-1}$ <sup>[17]</sup> and the  $d_{31}$  from **Figure 7a** can be used to calculate the predicted values of  $v'/v_0$  and  $\kappa'/\kappa_0$  which correspond to the initial sample depicted in **Figures 3 and 4**. This treatment can be extended to the stable trace in **Figure 5**, using the  $d_{31}$  value of  $-476 \text{ pC N}^{-1}$  calculated from the measurement shown in **Figure 7b** and the literature value of  $d_{33} = 2400 \text{ pC N}^{-1}$ .<sup>[17]</sup> We can

continue this to include the STO sample corresponding to the experiment shown in **Figure 8**. **Table 2** provides a comprehensive overview.

**Table 2.** Material type, properties, predicted and measured  $v'/v_0$  and  $\kappa'/\kappa_0$  values for PZT, fresh PMN-33PT, cycled PMN-33PT and STO.

					Predicted	Measured	
Material	Type	$d_{33}$ [pC N <sup>-1</sup> ]	$d_{31}$ [pC N <sup>-1</sup> ]	$\gamma$	$-\gamma(d_{33} + 2d_{31})$ [m V <sup>-1</sup> ]	$v'/v_0$ [m V <sup>-1</sup> ]	$\kappa'/\kappa_0$ [m V <sup>-1</sup> ]
PZT	FE	435 <sup>[22]</sup>	-100 <sup>[23]</sup>	15 <sup>[21]</sup>	$-3.5 \times 10^{-9}$ <sup>[3]</sup>	$-3.3 \times 10^{-9}$ <sup>[3]</sup>	$-9.5 \times 10^{-9}$ <sup>[3]</sup>
PMN-33PT (fresh)	RFE	1225 <sup>[17]</sup>	-1327	15 <sup>[21]</sup>	$2.1 \times 10^{-8}$	$2.6 \times 10^{-8}$	$3.9 \times 10^{-8}$
PMN-33PT (cycled)	RFE	2400 <sup>[17]</sup>	-476	15 <sup>[21]</sup>	$-2.2 \times 10^{-8}$	-	$-3.9 \times 10^{-7}$
STO	PE	100 <sup>[24]</sup>	-8.4 <sup>[25]</sup>	1.5 <sup>[26]</sup>	$-9.6 \times 10^{-11}$	$-1 \times 10^{-10}$	$-2 \times 10^{-10}$

We see that the initial results on fresh PMN-33PT and STO are quantitatively explained by **Equations (1)** and **(2)** without adjustable parameters, just as the case for PZT. Comparing the sound velocity and thermal conductivity results from **Figures 3** and **4** to that of PZT, we do indeed see the resulting curves of PMN-33PT invert, and that the latter are an order of magnitude larger. The summation of the piezoelectric coefficients ( $d_{33} + 2d_{31}$ ) of PMN-33PT has the opposite sign than that of PZT,<sup>[3]</sup> leading to the sign inversion in the sensitivity of sound velocity and thermal conductivity to field. This strongly confirms the theory that the dispersion of acoustic phonons is affected by an external electric field and further, that acoustic phonons can thus be considered as

ferrons carrying polarization, since they are strain-coupled to the optical phonons. The second sign inversion, between cycled (**Figure 5**) and non-cycled (**Figure 4a**) PMN-33PT is also predicted by the change in piezoelectric coefficients but not the additional increase in sensitivity by an order of magnitude. However, this does not invalidate the theory, since we used the literature value for  $d_{33}$ . As the sample's geometry was not amenable to a direct measurement, we had no experimental access to  $d_{33}$ . To calculate the cycled sample's predicted values, we used the value for  $d_{33}$  documented in the literature<sup>[17]</sup> for a sample subjected to a 1 Hz AC voltage for 40 cycles; it is well reported that ferroelectric relaxors have complex chemistry and competing energy scales at the microscopic scale.<sup>[20]</sup>

Regarding **Figures 4 b-d**, we pose that the variation of behavior is related to the changes in piezoelectric coefficients as the material experienced multiple rounds of poling processes. In Reference Negi et al.,<sup>[17]</sup> PMN-PT was poled in an AC field at various frequencies and in a DC voltage held for various times and afterwards,  $d_{33}$  was measured. Two samples DC poled at fields of  $1.25 \times 10^5 \text{ V m}^{-1}$  for 120 s and 200 s had  $d_{33}$  values of 505 and 1175  $\text{pC N}^{-1}$ , respectively, and another sample poled at  $5 \times 10^5 \text{ V m}^{-1}$  for 200 s had a  $d_{33}$  value of 1430  $\text{pC N}^{-1}$ . It is unclear if these are the first poling procedures on the samples; however, we can see the range that the piezoelectric coefficient can vary under these changes in poling conditions. The same paper shows data for a sample cycled through 3 times in a DC field of  $4 \times 10^5 \text{ V m}^{-1}$  held at 150 s. The  $d_{33}$  changes minimally from 1515 to 1481  $\text{pC N}^{-1}$ . Perhaps this helps explain the stable transition that occurs after multiple rounds of poling. Also in that investigation, an electric field of  $5 \times 10^5 \text{ V m}^{-1}$  was sustained at a frequency of 1 Hz. Following a single cycle of poling, the  $d_{33}$  value was reported at 1225  $\text{pC N}^{-1}$ . Remarkably, after 40 cycles, this value surged to 2400  $\text{pC N}^{-1}$ , signifying a remarkable increase in the  $d_{33}$  parameter. These  $d_{33}$  values were used to calculate the predicted value of  $v'/v_0$  for the fresh sample 1 and cycled sample 2, respectively, shown in **Table 2**.

### 3. Conclusion

In summary, our study involved measuring thermal conductivity and sound velocity of PMN-33PT on two distinct samples. The first sample exhibited values consistent with theoretical predictions based on the ferron theory and specific piezoelectric coefficients. The second sample,

subjected more than 10 times to a sweeping electric field, displayed a sign change in  $\kappa'/\kappa_0$  compared to the results obtained in the fresh sample, and another increase by an order of magnitude, which suggested alterations in piezoelectric coefficients. We could only measure  $d_{31}$  on our samples due to instrument limitations and sample thickness. Interestingly, the summation ( $d_{33} + 2d_{31}$ ) exhibited differing signs and values between PZT and PMN-33PT, and then a second sign change between the electrically cycled and the fresh samples of PMN-33PT. Calculated  $\kappa'/\kappa_0$  values using measured  $d_{31}$  aligned with expected piezoelectric coefficient changes. Though a magnitude difference in the second sample may relate to using samples with different histories, further investigation is necessary. Additionally, our study on STO under electric field showed almost no change in thermal conductivity or sound velocity, reinforcing the necessity of a remnant moment for ferronic behavior in ferroelectrics. Comparing PMN-33PT with Wooten et al.'s<sup>[3]</sup> findings for PZT indicates a stronger signal under electric field, suggesting promising applications despite the need for further signal enhancement in studies on thermal switches.

#### 4. Experimental Section

PMN-33PT samples with poling direction of (001) were obtained from MSE Supplies and STO samples with the same orientation were obtained from Princeton Scientific Corps. Silver epoxy (EpoTek) was applied to the sides of the STO wafer to act as electrodes. To apply an electric field to PMN-33PT, 10 nm of Ti then 90 nm of Au was evaporated onto the primary surfaces in a CHA solution system E-gun evaporator.

To measure the sound velocity, a fresh sample was cleaved into parallelepiped of approximate size 3 mm  $\times$  1 mm  $\times$  0.5 mm. Coiled Cu wires (Omega, diameter of 25  $\mu$ m) were attached to the electrodes to apply an electric field. Voltage was applied using a Stanford Research Systems' Data Precision 8200. The targeted longitudinal resonant frequency was calculated using the Young's modulus, density provided from manufacturer's website, and sample dimensions. The sample was placed in a Resonant Ultrasound Spectrometer (RUS) (Alamo Creek Engineering). In the RUS, the sample was subjected to ultrasound frequencies that were amplified if they corresponded to a natural resonant frequency. The peak corresponding to the longitudinal frequency shifted with applied voltage and was tracked by hand.



Thermal conductivity measurements were conducted using the static heater-and-sink method on two samples. Two type T thermocouples consisting of a copper and constantan wire were adhered to the first sample using GE Varnish, which is thermally conducting but electrically insulating. This ensured no short circuiting to the electrodes occurred. On the second sample StyCast epoxy was used instead of GE varnish which is also thermally conducting but electrically insulating. Sample 1 was subsequently positioned on an alumina base, serving as a heat sink, and secured with GE varnish, while sample 2 was affixed using StyCast. A strain gauge was placed with GE varnish on sample 1 and with StyCast on sample 2 acting as the heater. Both samples were then placed in a vacuumed environment inside a Lakeshore nitrogen-cooled cryostat. The temperature was allowed to stabilize for at least one hour. Given its paraelectric nature, thermal conductivity of STO was measured in field without any prior poling protocols. During the measurements, the electric field was maintained for about 5 minutes before the thermal conductivity was recorded to alleviate any pyroelectric artifacts.

To determine the  $d_{31}$  coefficient, we tracked the displacement of the top surface of the sample as a function of applied AC field. The sample measuring approximately  $10 \text{ mm} \times 10 \text{ mm} \times 0.5 \text{ mm}$  was securely affixed to a microscope glass slab using GE varnish. As the top surface was smaller than the laser spot size, a piece of Kapton tape was placed atop the sample. This layer provided a broader area for laser-beam to hit the edge of the sample ensuring smaller measurement error. For this displacement measurement, we relied on the Keyence LKG32 Laser Sensor. To apply the AC voltage, we employed the Techron 5050 Linear Amplifier in tandem with the Agilent 33120A Waveform Generator. Throughout the experiment, we continuously monitored the changes in displacement using the Rigol MSO5074 oscilloscope.

A parallel experiment was carried out using a cycled sample. The objective of this second experiment was to elucidate the impact of cycling the sample through several sweeps of the electric field. The mounting of the sample for this experiment was slightly different from the first measurement. The laser beam hit the strain gauge placed on the top of the sample to measure the longitudinal displacement while applying electric field. The  $d_{31}$  coefficient was calculated by taking the slope of strain vs electric field plots.

## Acknowledgements

The primary funding for this work (DR, JPH) is from the US National Science Foundation grant CBET 213 3718. BLW is supported by a US Department of Defense SMART fellowship. The authors thank the OSU Smart Materials and Structures Lab, specifically Mohid Khattak who assisted in  $d_{31}$  measurements. The authors thank Prof. Patrick Woodward for engaging discussion involving relaxor ferroelectric materials. Metallization was conducted at OSU's Nanotech West Lab; the authors thank the lab manager, Paul Steffan, for the detailed training and guidance.

## Conflicts of Interest

The authors declare no conflicts of interest.

## Data Availability Statement

The data supporting the findings presented in this article are available from the corresponding authors upon reasonable request.

## Bibliography

- [1] Polarization Transport in Ferroelectrics, G. E. W. Bauer, P. Tang, R. Iguchi, J. Xiao, K. Shen, Z. Zhong, T. Yu, S. M. Rezende, J. P. Heremans, K. Uchida, American Physical Society, **2023**, DOI: 10.1103/PhysRevApplied.20.050501.
- [2] G. E. W. Bauer, R. Iguchi, K. Uchida, *Phys Rev Lett* **2021**, 126.
- [3] B. L. Wooten, R. Iguchi, P. Tang, J. S. Kang, K.-I. Uchida, G. E. W. Bauer, J. P. Heremans, 'Electric field-dependent phonon spectrum and heat conduction in ferroelectrics', **2023**.
- [4] G. Wehmeyer, T. Yabuki, C. Monachon, J. Wu, C. Dames, *Appl Phys Rev* **2017**, 4, DOI: 10.1063/1.5001072.
- [5] C. "Liu, C. 'Wu, Y. 'Zhao, Z. 'Chen, T.-L. 'Ren, Y. 'Chen, G. 'Zhang, *Physics Reports - To be published* **2024**.
- [6] J. F. Ihlefeld, B. M. Foley, D. A. Scrymgeour, J. R. Michael, B. B. McKenzie, D. L. Medlin, M. Wallace, S. Trolrier-Mckinstry, P. E. Hopkins, *Nano Lett* **2015**, 15, 1791, DOI: 10.1021/nl504505t.
- [7] M. Davis, D. Damjanovic, N. Setter, *Phys Rev B Condens Matter Mater Phys* **2006**, 73, DOI: 10.1103/PhysRevB.73.014115.
- [8] Z. Kutnjak, R. Blinc, Y. Ishibashi, *Phys Rev B Condens Matter Mater Phys* **2007**, 76, DOI: 10.1103/PhysRevB.76.104102.

- [9] H. H. Wu, R. E. Cohen, *Phys Rev B* **2017**, *96*, DOI: 10.1103/PhysRevB.96.054116.
- [10] J. Peräntie, J. Hagberg, A. Uusimäki, J. Tian, P. Han, *J Appl Phys* **2012**, *112*, DOI: 10.1063/1.4745902.
- [11] J. Fan, X. Lu, W. Cao, *J Alloys Compd* **2020**, *835*, DOI: 10.1016/j.jallcom.2020.155171.
- [12] M. Sulc, M. Pokorny, *Journal de Physique IV (Proceedings)* **2005**, *126*, 77, DOI: 10.1051/jp4:2005126016.
- [13] J. A. Lima, W. Paraguassu, P. T. C. Freire, A. G. Souza filho, C. W. A. Paschoal, J. M. Filho, A. L. Zanin, M. H. Lente, D. Garcia, J. A. Eiras, *Journal of Raman Spectroscopy* **2009**, *40*, 1144, DOI: 10.1002/jrs.2247.
- [14] K. Fang, W. Jing, F. Fang, *Journal of the American Ceramic Society* **2019**, *102*, 7710, DOI: 10.1111/jace.16667.
- [15] Y. Zhou, Q. Li, C. Xu, F. Zhuo, D. Liu, Q. Yan, Y. Zhang, X. Chu, *J Appl Phys* **2019**, *126*, DOI: 10.1063/1.5097681.
- [16] K. K. Rajan, M. Shanthi, W. S. Chang, J. Jin, L. C. Lim, *Sens Actuators A Phys* **2007**, *133*, 110, DOI: 10.1016/j.sna.2006.03.036.
- [17] A. Negi, H. P. Kim, Z. Hua, A. Timofeeva, X. Zhang, Y. Zhu, K. Peters, D. Kumah, X. Jiang, J. Liu, *Advanced Materials* **2023**, *35*, DOI: 10.1002/adma.202211286.
- [18] M. Otoničar, A. Bradeško, L. Fulanović, T. Kos, H. Uršič, A. Benčan, M. J. Cabral, A. Henriques, J. L. Jones, L. Riemer, D. Damjanovic, G. Dražić, B. Malič, T. Rojac, *Adv Funct Mater* **2020**, *30*, DOI: 10.1002/adfm.202006823.
- [19] F. Li, S. Zhang, T. Yang, Z. Xu, N. Zhang, G. Liu, J. Wang, J. Wang, Z. Cheng, Z. G. Ye, J. Luo, T. R. Shrout, L. Q. Chen, *Nat Commun* **2016**, *7*, DOI: 10.1038/ncomms13807.
- [20] T. Rojac, *Commun Mater* **2023**, *4*, DOI: 10.1038/s43246-023-00336-9.
- [21] Y. Fu, D. J. Singh, *Phys Rev Mater* **2018**, *2*, 1, DOI: 10.1103/PhysRevMaterials.2.094408.
- [22] Materials Technical Data (Typical Values), <https://info.piezo.com/hubfs/Data-Sheets/piezo-material-properties-data-sheet-20201112.pdf>.
- [23] I. Kanno, S. Fujii, T. Kamada, R. Takayama, *Appl Phys Lett* **1997**, *70*.
- [24] B. Khanbabaee, E. Mehner, C. Richter, J. Hanzig, M. Zschornak, U. Pietsch, H. Stöcker, T. Leisegang, D. C. Meyer, S. Gorfman, *Appl Phys Lett* **2016**, *109*, DOI: 10.1063/1.4966892.
- [25] A. Erba, K. E. El-Kelany, M. Ferrero, I. Baraille, M. Rérat, *Phys Rev B Condens Matter Mater Phys* **2013**, *88*, DOI: 10.1103/PhysRevB.88.035102.
- [26] A. G. Beattie, G. A. Samara, *J Appl Phys* **1971**, *42*, 2376, DOI: 10.1063/1.1660551.